Supplementary Materials and Methods for:

Western diet consumption impairs memory function via dysregulated hippocampus acetylcholine signaling

Anna M. R. Hayes[1], Logan Tierno Lauer[1], Alicia E. Kao[1], Shan Sun[2], Molly E. Klug[1], Linda Tsan[1,3], Jessica J. Rea[1,3], Keshav S. Subramanian[1,3], Cindy Gu[1], Natalie Tanios[1], Arun Ahuja[1], Kristen N. Donohue[1], Léa Décarie-Spain[1], Anthony A. Fodor[2], Scott E. Kanoski[1,3]†

[1]Human and Evolutionary Biology Section, Department of Biological Sciences, University of Southern California, Los Angeles, CA, USA

[2]Department of Bioinformatics and Genomics, University of North Carolina at Charlotte, Charlotte, NC, USA

[3]Neuroscience Graduate Program, University of Southern California, Los Angeles, CA, USA

Corresponding author:

†Scott E. Kanoski

Current Address: 3616 Trousdale Parkway, AHF-252, Los Angeles, CA 90089-0372

E-mail: kanoski@usc.edu

Telephone number: (213) 821-5762

Dietary model – part 2

Experimental cohort 1: Early life cafeteria (CAF) diet followed by healthy diet intervention: behavioral and metabolic outcomes. Rats (n=24 total) received either the CAF or CTL diet from PN 26-86 (n=12 per group). The 30-day early life diet period encompassed PN 26-56, after which point behavioral testing occurred while rats remained on their respective diets (Fig. 1A). Behavioral tests began with Novel Object Recognition (NOR) and Novel Location Recognition (NLR) experiments conducted in a counterbalanced fashion by diet group on PN 60-61 (with habituation on PN 59). Rats then were tested in the Novel Object in Context (NOIC) task from PN 68-70 (with habituation on PN 66 and 67). Zero Maze and Open Field tests were performed on PN 74 and PN 75, respectively. An intraperitoneal glucose tolerance test (IPGTT) was conducted on PN 77, and rats on the CAF diet were switched to the standard healthy chow diet (i.e., the same diet that the CTL group received throughout the study) on PN 86. All the outcomes measured up to PN 86 are considered the assessments "before the healthy diet intervention." The 30-day healthy diet intervention period for the CAF rats lasted from PN 86-116. For the outcomes assessed after the healthy diet intervention, NOIC was performed from PN 125-127 (habituation on PN 123 and 124), body composition was analyzed on PN 132, NOR was performed on PN 136, Zero Maze was conducted on PN 140, NLR was assessed on PN 143, and an IPGTT was performed on PN 147. Fecal samples were collected for 16s rRNA sequencing analyses of the gut microbiome on PN 56 and PN 116. Tissue was harvested on PN 150.

Experimental cohort 2: Early life CAF diet without healthy diet intervention: tissue collection. Rats in this cohort (n=24 total) received either CAF diet or standard chow diet as control (CTL) from PN 26-74 (n=12 per group), with NOIC testing from PN 68-70 (with habituation on PN 66 and 67) followed by tissue harvest at PN 74. Through this cohort, we were able to

collect cecal content (which is a terminal endpoint) following CAF exposure without a healthy diet intervention.

Experimental cohort 3: Early life CAF diet followed by healthy diet intervention: in vivo fiber photometry ACh release analyses. Rats (n=24 total) received either CAF diet or standard chow diet as control (CTL) from PN 26-56 (n=12 per group). The 30-day early life diet period encompassed PN 26-56, as in previous cohorts, but the CAF group was switched onto the healthy standard chow at PN 56 to mark the beginning of the healthy diet intervention period. Body composition measures were also performed on PN 56. Stereotaxic surgeries for *in vivo* fiber photometry analyses were performed on PN 67, PN 71, and PN 72 (n=8 rats per day, counterbalanced per group). This timing was selected to allow the CAF rats to acclimate to the standard healthy chow for 10+ days before surgery as well as for adequate recovery time before behavior testing while also accommodating for 30+ days of the healthy diet intervention period before behavior testing. NOIC was performed in squads from PN 95-125. Rats from this cohort were transcardially perfused on PN 226 and brain tissue was harvested for histological confirmation of AAV injection placement.

Experimental cohort 4: Early life CAF diet followed by healthy diet intervention: ACh pharmacology. Rats in this cohort (n=30 total) all received CAF diet from PN 26-56, but they were assigned to different groups at PN 26 according to which ACh agonist they would receive during NOIC behavior testing (n=10 per group). The 30-day early life diet period encompassed PN 26-56, as in previous cohorts, but the CAF group was switched onto the healthy standard chow at PN 56 to mark the beginning of the healthy diet intervention period. Stereotaxic surgeries to install bilateral indwelling cannulae into the dorsal HPC

were performed on PN 66-69 (n=8 rats per day, counterbalanced per group). This surgery timing was selected to allow the CAF rats to acclimate to the standard healthy chow for 10+ days before surgery as well as for adequate recovery time before behavior testing while also accommodating for 30+ days of the healthy diet intervention period before neuropharmacological behavior testing. NOIC was performed from PN 94-96 (habituation on PN 92 and 93). Rats from this cohort were infused with blue sky ink through their cannulae on PN 109 as described below and immediately euthanized to enable validation of infusion sites.

Metabolic assessments

Body composition. Nuclear magnetic resonance (NMR) was used to quantify body composition as previously described (Davis et al., 2020; Tsan et al., 2022b) both immediately after the 30-d CAF diet period in early life (PN 56) as well as after the 30-d healthy diet intervention in adulthood (PN 132). Briefly, rats were food-restricted for 1 h, weighed, and scanned using the Bruker NMR Minispec LF 90II (Bruker Daltonics, Inc., Billerica, MA, USA) interfaced to a computer equipped with Minispec Plus 4.1.5 software. This system employs time-domain NMR signals from all protons to quantify body composition and is advantageous because it is non-invasive and does not require administration of anesthesia. The ratio of fat-to-lean mass per subject was calculated as [fat mass (g) / lean mass (g)].

Glucose tolerance. An intraperitoneal glucose tolerance test (IPGTT) was performed to examine glucose metabolism both immediately after the 30-d CAF diet period in early life (PN 77) as well as after the 30-d healthy diet intervention in adulthood (PN 147). Rats were food-restricted 22 h prior to the test, following established procedures (Hayes et al., 2022;

Tsan et al., 2022a; Tsan et al., 2022b). Blood was sampled from the tip of the tail for baseline blood glucose readings (fasted state) and all subsequent blood glucose readings and measured using a glucometer (One Touch Ultra2, LifeScan, Inc., Milpitas, CA, USA). Following the baseline reading, each rat received an intraperitoneal (IP) injection of a 50% glucose solution (1 g/kg body weight; Dextrose anhydrous, VWR Chemicals, LLC, Solon, OH, USA). Aside from the baseline reading (collected immediately before injection), blood glucose readings were subsequently obtained at the 30, 60, 90, and 120 min time points following injection. Area under the curve was calculated using the trapezoidal rule with 0 mg/dL set as the mathematical “baseline”.

Behavioral assessments – part 2

Novel Object Recognition (NOR). NOR was used to evaluate exploration of novelty in the form of a novel object, which under testing parameters employed is perirhinal cortex-dependent and not HPC-dependent (Albasser et al., 2011). A grey opaque box (38.1 cm L × 56.5 cm W × 31.8 cm H), placed in a dimly lit room in which two adjacent desk lamps were pointed toward the floor, was used as the NOR apparatus. Procedures followed as described in (Noble et al., 2021), modified from (Beilharz et al., 2014). Rats were habituated to the empty apparatus and conditions for 10 min 1-2 days prior to testing. The test consisted of a 5-min familiarization phase during which rats were placed in the center of the apparatus (facing a neutral wall to avoid biasing them toward either object) with two identical objects and allowed to explore. The objects used were either two identical cans or two identical stem-less wine glasses (first NOR time point), or two identical tin canisters (with tin covers) or two identical ceramic vases (second NOR time point). Rats were then removed from the apparatus and placed in their home cage for 5 min. During this period, the apparatus and objects were cleaned with 10% ethanol solution and one of the objects

was replaced with a different one (for time point 1: either the can or glass – whichever the animal had not previously been exposed to – i.e., the “novel object”; for time point 2: either the tin canister or vase – whichever the animal had not previously been exposed to – i.e., the “novel object”). Rats were then placed in the center of the apparatus again and allowed to explore for 3 min. The novel object and side on which the novel object was placed were counterbalanced per treatment group. The time each rat spent exploring the objects was quantified by hand-scoring of video recordings by an experimenter blinded to the animal group assignments. Object exploration was defined as the rat sniffing or touching the object with the nose or forepaws.

Zero Maze. Following established procedures (Noble et al., 2021; Tsan et al., 2022a; Tsan et al., 2022b), the Zero Maze procedure was used to examine anxiety-like behavior. The Zero Maze apparatus consisted of an elevated circular track (11.4 cm wide track, 73.7 cm height from track to the ground, 92.7 cm exterior diameter) that is divided into four equal length segments: two sections with 3-cm high curbs (open), and two sections with 17.5 cm high walls (closed). Ambient lighting was used during testing. Rats were placed in the maze on an open section of the track and allowed to roam for 5 min, during which time they could freely ambulate through the different segments of the track. The apparatus was cleaned with 10% ethanol between rats. The time each rat spent in the open segments of the track (defined as the center of the rat in an open arm) as well as the number of entries into the open segments of the track were measured via video recording using ANYmaze activity tracking software (Stoelting Co., Wood Dale, IL, USA).

Open Field. Open Field was performed to test for locomotor activity as well as anxiety-like behavior following previous procedures (Belzung and Griebel, 2001; Hayes et al., 2022;

Noble et al., 2021; Suarez et al., 2018). The Open Field apparatus was a gray arena (53.5 cm L × 54.6 cm W × 36.8 H) with a designated center zone within the arena (19 cm × 17.5 cm). The center zone was maintained under diffused lighting (44 lux) compared to the corners and edges (~30 lux). For testing, rats were placed in the center of the apparatus and allowed to freely explore for 10 min. The apparatus was cleaned with 10% ethanol between rats. Video recording using ANYmaze activity tracking software (Stoelting Co., Wood Dale, IL, USA) was used to quantify time spent in the center zone (a measuring of anxiety-like behavior) and distance travelled in the apparatus during the task (locomotor activity).

Stereotaxic surgery

Intracranial viral injection and in vivo photometry optic fiber placement. Rats were anesthetized and sedated via intramuscular injections of a cocktail of ketamine (90.1 mg/kg body weight), xylazine (2.8 mg/kg body weight), and acepromazine (0.72 mg/kg body weight), followed by a pre-operative subcutaneous injection of analgesic (buprenorphine SR, 1.0 mg/kg body weight). Upon sedation, the surgical site was shaved and prepared with iodine and ethanol swabbing. The animals were then placed in a stereotaxic apparatus. The iAChSnFR adeno-associated virus (AAV; 1 µL; original titer ≥ 7×10^{12} vg/mL diluted 1:2 with artificial cerebral spinal fluid; pAAV.hSynap.iAChSnFR, 137950-AAV1, Addgene, Watertown, MA, USA), validated as a selective in vivo ACh sensor in rodents (Borden et al., 2020; Chen et al., 2021; Lin et al., 2021; Nichols et al., 2022; Zhu et al., 2020), was delivered into the dorsal dentate gyrus of the HPC (anterior/posterior [A/P]: -3.24; medial/lateral [M/L]: +/-1.80; dorsal/ventral [D/L]: -3.50; with 0 as the reference point at bregma for A/P, M/L, and D/L) using a microinfusion pump (Harvard Apparatus, Cambridge, MA, USA) equipped with a 33-gauge microsyringe injector connected to a PE20 catheter

and Hamilton syringe. The injection flow rate was set to 5 µL/min. To allow for complete delivery of infusate, injectors were kept in place for 2 min post-injection. Fiber optic cannulae (flat 400 µm core, 0.48 numerical aperture, 5mm; Doric Lenses Inc., Quebec, Canada) were implanted in the dorsal dentate gyrus at the same coordinates as the viral infusion (A/P: -3.24; M/L: +/-1.80; D/L: -3.50; with 0 as the reference point at bregma for A/P, M/L, and D/L). Optic fibers were then affixed to the skull with jeweler's screws, instant adhesive super glue, and dental cement.

Bilateral indwelling cannulae in HPC. Intramuscular injections of a cocktail of ketamine (90.1 mg/kg body weight), xylazine (2.8 mg/kg body weight), and acepromazine (0.72 mg/kg body weight), followed by a pre-operative subcutaneous injection of analgesic (buprenorphine SR, 1.0 mg/kg body weight) were administered to anesthetize and sedate rats. The surgical site was shaved and prepared with iodine and ethanol swabbing, and subsequently the animals were situated in a stereotaxic apparatus. Indwelling bilateral guide cannulae (26-gauge, Plastics One, Protech International Inc., Boerne, TX, USA) were then placed targeting the dorsal HPC (A/P: -4.08; M/L: +/-2.50; D/L: -2.60; with 0 as the reference point at bregma for A/P, M/L, and D/L). Cannulae were fastened to the skull with jeweler's screws, instant adhesive super glue, and dental cement. Obturators were secured in the cannulae to prevent blockage until experimentation.

Immunohistochemistry

Following tissue fixation and sectioning, general fluorescence immunohistochemistry (IHC) was performed. To amplify the native GFP signal for dorsal dentate gyrus ACh sensor injection site histology, a chicken anti-GFP primary antibody (1:500, Abcam, catalog # ab13970) was used followed by a donkey anti-chicken secondary antibody conjugated to

AF488 (1:500, Jackson Immunoresearch, RRID: AB_2340375). Antibodies were prepared in 0.02M potassium phosphate buffered saline (KPBS) solution containing 0.2% bovine serum albumin and 0.3% Triton X-100. Sections from Swanson Brain Atlas levels 27-33 (Swanson, 2018) were incubated in the primary antibody solution at 4°C overnight. Upon thorough washing with 0.02M KPBS the subsequent day, sections were incubated in the secondary antibody at 4°C overnight. Sections were then mounted and coverslipped using 50% glycerol in 0.02M KPBS, and the edges were sealed with clear nail polish. Photomicrographs were captured using a Nikon 80i camera (Nikon DSQI1, 1280X1024 resolution, 1.45 megapixel) under epifluorescence.

Microbiome analyses

Fecal collection. Fecal collections were performed on PN 56 and 116 from the first experimental cohort. Rats were placed into a sterile cage (without bedding) and mildly restrained until defecation. Two fecal samples per rat per time point were collected. Each was weighed immediately upon defecation under sterile conditions and placed into a distinct Dnase/Rnase-free 2 mL cryogenic vial and immediately embedded in dry ice (one sample per vial). All samples were then stored in a -80°C freezer until further analysis. Between every rat, all cages and sample collection materials were thoroughly cleaned with 70% ethanol. All fecal collections were performed between 12:00 and 15:00 (during the dark cycle).

Cecal content collection. Collecting cecal content is a terminal procedure, and thus it was performed on the terminal tissue collection days for the first two experimental cohorts (PN 150 and PN 74, respectively). Following euthanasia procedures (described above), an abdominal incision was made to expose the intestines. The cecum was identified and a

small incision was made therein. Cecal content was then collected directly into a pre-tared Dnase/Rnase-free 2 mL cryogenic vial, weighed, and immediately embedded into dry ice. All samples were then stored in a -80°C freezer until further analysis. Two vials of cecal content were collected per rat. Between every rat, all cecal content collection materials were thoroughly cleaned with 70% ethanol. Cecal content collections were performed between 11:00 and 17:00 (during the dark cycle).

Sample processing and 16S rRNA sequencing. Bacterial genomic DNA was extracted from fecal samples using Laragen Inc.'s validated in-house fecal DNA extraction protocol. Quantification of 16S rRNA gene loads was performed by qPCR using the SYBR Green master mix (Roche, Basel, Switzerland), universal 16S rRNA gene primers55, and the QuantStudio 5 thermocycler (cycling parameters: 2 min at 50 °C, 10 min at 95 °C, 40 cycles of 10 s at 95 °C, and 45 s at 62 °C). Sequencing libraries were generated using previously established methods (Caporaso et al., 2011). The V4 regions of the 16S rRNA gene were PCR amplified using individually barcoded universal primers and 3 ng of the extracted genomic DNA. The PCR reaction was set up in a single reaction, and the PCR product was purified using Laragen Inc.'s validated in-house bead-based purification. Purified PCR product from each sample (250 ng) was pooled and sequenced by Laragen, Inc., using the Illumina MiSeq platform and 2 × 150 bp reagent kit for paired-end sequencing.

Microbiome data processing and analysis. The 16S rRNA amplicon sequences were analyzed with DADA2 and QIIME2 following the developers' instructions (Bolyen et al., 2019; Callahan et al., 2016). The forward reads were truncated to 120 bp and denoised with DADA2 to 2,162 amplicon sequence variants (ASV). Chimeras were removed with the 'consensus' method using DADA2. The ASVs were classified with 'classify-sklearn' in

QIIME2 using the SILVA database (release 138). The taxonomic abundance tables were normalized as previously described (Jones et al., 2018) to correct for different sequencing depth across samples. Statistical analyses were performed with R (4.2.0). The Bray-Curtis dissimilarity between samples were calculated using the genus level abundance and visualized using the principal coordinates analysis (PCoA) with function 'capscale' in R package 'vegan'. The associations of microbial community profiles and diet were analyzed with the PERMANOVA test using the function 'adonis' in the same package. Shannon index was used for analyzing alpha-diversity. Wilcoxon rank sum test was used to analyze the associations of individual taxa and diet. Taxa with presence in less than 25% samples were excluded to avoid spurious associations. P-values were adjusted with the Benjamini-Hochberg method for multiple hypotheses testing. The significant taxa (FDR<0.1) were highlighted in the phylogenetic tree using R package 'plotmicrobiome'. The associations of taxa and NOIC were analyzed with Spearman's correlations.

Machine learning – predicting NOIC performance using microbiome. Machine learning approaches were used to test if NOIC memory performance measures could be predicted from gut microbiome profiles after the WD access period but before the healthy diet intervention. Random forest regression models were built with R package 'randomForest' to predict NOIC and NLR from the taxonomic abundance at the genus level. Performance of the models were evaluated with 3-fold and 4-fold cross validation.

Supplementary References

Albasser, M.M., Amin, E., Iordanova, M.D., Brown, M.W., Pearce, J.M., Aggleton, J.P., 2011. Perirhinal cortex lesions uncover subsidiary systems in the rat for the detection of novel and familiar objects. European Journal of Neuroscience 34, 331-342.

Beilharz, J.E., Maniam, J., Morris, M.J., 2014. Short exposure to a diet rich in both fat and sugar or sugar alone impairs place, but not object recognition memory in rats. Brain, Behavior, and Immunity 37, 134-141.

Belzung, C., Griebel, G., 2001. Measuring normal and pathological anxiety-like behaviour in mice: a review. Behavioural Brain Research 125, 141-149.

Bolyen, E., Rideout, J.R., Dillon, M.R., Bokulich, N.A., Abnet, C.C., Al-Ghalith, G.A., Alexander, H., Alm, E.J., Arumugam, M., Asnicar, F., Bai, Y., Bisanz, J.E., Bittinger, K., Brejnrod, A., Brislawn, C.J., Brown, C.T., Callahan, B.J., Caraballo-Rodríguez, A.M., Chase, J., Cope, E.K., Da Silva, R., Diener, C., Dorrestein, P.C., Douglas, G.M., Durall, D.M., Duvallet, C., Edwardson, C.F., Ernst, M., Estaki, M., Fouquier, J., Gauglitz, J.M., Gibbons, S.M., Gibson, D.L., Gonzalez, A., Gorlick, K., Guo, J., Hillmann, B., Holmes, S., Holste, H., Huttenhower, C., Huttley, G.A., Janssen, S., Jarmusch, A.K., Jiang, L., Kaehler, B.D., Kang, K.B., Keefe, C.R., Keim, P., Kelley, S.T., Knights, D., Koester, I., Kosciolek, T., Kreps, J., Langille, M.G.I., Lee, J., Ley, R., Liu, Y.-X., Loftfield, E., Lozupone, C., Maher, M., Marotz, C., Martin, B.D., McDonald, D., McIver, L.J., Melnik, A.V., Metcalf, J.L., Morgan, S.C., Morton, J.T., Naimey, A.T., Navas-Molina, J.A., Nothias, L.F., Orchanian, S.B., Pearson, T., Peoples, S.L., Petras, D., Preuss, M.L., Pruesse, E., Rasmussen, L.B., Rivers, A., Robeson, M.S., Rosenthal, P., Segata, N., Shaffer, M., Shiffer, A., Sinha, R., Song, S.J., Spear, J.R., Swafford, A.D., Thompson, L.R., Torres, P.J., Trinh, P., Tripathi, A., Turnbaugh, P.J., Ul-Hasan, S., Van Der Hooft, J.J.J., Vargas, F., Vázquez-Baeza, Y., Vogtmann, E., Von Hippel, M., Walters, W., Wan, Y., Wang, M., Warren, J., Weber, K.C., Williamson, C.H.D., Willis, A.D., Xu, Z.Z., Zaneveld, J.R., Zhang, Y., Zhu, Q., Knight, R., Caporaso, J.G., 2019. Reproducible, interactive, scalable and extensible microbiome data science using QIIME 2. Nature Biotechnology 37, 852-857.

Borden, P.M., Zhang, P., Shivange, A.V., Marvin, J.S., Cichon, J., Dan, C., Podgorski, K., Figueiredo, A., Novak, O., Tanimoto, M., Shigetomi, E., Lobas, M.A., Kim, H., Zhu, P.K., Zhang, Y., Zheng, W.S., Fan, C., Wang, G., Xiang, B., Gan, L., Zhang, G.-X., Guo, K., Lin, L., Cai, Y., Yee, A.G., Aggarwal, A., Ford, C.P., Rees, D.C., Dietrich, D., Khakh, B.S., Dittman, J.S., Gan, W.-B., Koyama, M., Jayaraman, V., Cheer, J.F., Lester, H.A., Zhu, J.J., Looger, L.L., 2020. A fast genetically encoded fluorescent sensor for faithful in vivo acetylcholine detection in mice, fish, worms and flies. Cold Spring Harbor Laboratory.

Callahan, B.J., McMurdie, P.J., Rosen, M.J., Han, A.W., Johnson, A.J.A., Holmes, S.P., 2016. DADA2: High-resolution sample inference from Illumina amplicon data. Nature Methods 13, 581-583.

Caporaso, J.G., Lauber, C.L., Walters, W.A., Berg-Lyons, D., Lozupone, C.A., Turnbaugh, P.J., Fierer, N., Knight, R., 2011. Global patterns of 16S rRNA diversity at a depth of

millions of sequences per sample. Proceedings of the National Academy of Sciences 108, 4516-4522.

Chen, J., Cho, K.E., Skwarzynska, D., Clancy, S., Conley, N.J., Clinton, S.M., Li, X., Lin, L., Zhu, J.J., 2021. The Property-Based Practical Applications and Solutions of Genetically Encoded Acetylcholine and Monoamine Sensors. The Journal of Neuroscience 41, 2318-2328.

Davis, E.A., Wald, H.S., Suarez, A.N., Zubcevic, J., Liu, C.M., Cortella, A.M., Kamitakahara, A.K., Polson, J.W., Arnold, M., Grill, H.J., De Lartigue, G., Kanoski, S.E., 2020. Ghrelin Signaling Affects Feeding Behavior, Metabolism, and Memory through the Vagus Nerve. Current Biology 30, 4510-4518.e4516.

Hayes, A.M.R., Tsan, L., Kao, A.E., Schwartz, G.M., Décarie-Spain, L., Tierno Lauer, L., Klug, M.E., Schier, L.A., Kanoski, S.E., 2022. Early Life Low-Calorie Sweetener Consumption Impacts Energy Balance during Adulthood. Nutrients 14, 4709.

Jones, R.B., Zhu, X., Moan, E., Murff, H.J., Ness, R.M., Seidner, D.L., Sun, S., Yu, C., Dai, Q., Fodor, A.A., Azcarate-Peril, M.A., Shrubsole, M.J., 2018. Inter-niche and inter-individual variation in gut microbial community assessment using stool, rectal swab, and mucosal samples. Scientific Reports 8.

Lin, L., Gupta, S., Zheng, W.S., Si, K., Zhu, J.J., 2021. Genetically encoded sensors enable micro- and nano-scopic decoding of transmission in healthy and diseased brains. Molecular Psychiatry 26, 443-455.

Nichols, A.L., Blumenfeld, Z., Fan, C., Luebbert, L., Blom, A.E.M., Cohen, B.N., Marvin, J.S., Borden, P.M., Kim, C.H., Muthusamy, A.K., Shivange, A.V., Knox, H.J., Campello, H.R., Wang, J.H., Dougherty, D.A., Looger, L.L., Gallagher, T., Rees, D.C., Lester, H.A., 2022. Fluorescence activation mechanism and imaging of drug permeation with new sensors for smoking-cessation ligands. eLife 11, e74648.

Noble, E.E., Olson, C.A., Davis, E., Tsan, L., Chen, Y.-W., Schade, R., Liu, C., Suarez, A., Jones, R.B., De La Serre, C., Yang, X., Hsiao, E.Y., Kanoski, S.E., 2021. Gut microbial taxa elevated by dietary sugar disrupt memory function. Translational Psychiatry 11.

Suarez, A.N., Hsu, T.M., Liu, C.M., Noble, E.E., Cortella, A.M., Nakamoto, E.M., Hahn, J.D., De Lartigue, G., Kanoski, S.E., 2018. Gut vagal sensory signaling regulates hippocampus function through multi-order pathways. Nature Communications 9, 2181.

Swanson, L.W., 2018. Brain maps 4.0-Structure of the rat brain: An open access atlas with global nervous system nomenclature ontology and flatmaps. J Comp Neurol 526, 935-943.

Tsan, L., Chometton, S., Hayes, A.M.R., Klug, M.E., Zuo, Y., Sun, S., Bridi, L., Lan, R., Fodor, A.A., Noble, E.E., Yang, X., Kanoski, S.E., Schier, L.A., 2022a. Early life low-calorie sweetener consumption disrupts glucose regulation, sugar-motivated behavior, and memory function in rats. JCI Insight 7, e157714.

Tsan, L., Sun, S., Hayes, A.M.R., Bridi, L., Chirala, L.S., Noble, E.E., Fodor, A.A., Kanoski, S.E., 2022b. Early life Western diet-induced memory impairments and gut microbiome

changes in female rats are long-lasting despite healthy dietary intervention. Nutritional Neuroscience 25, 2490-2506.

Zhu, P.K., Zheng, W.S., Zhang, P., Jing, M., Borden, P.M., Ali, F., Guo, K., Feng, J., Marvin, J.S., Wang, Y., Wan, J., Gan, L., Kwan, A.C., Lin, L., Looger, L.L., Li, Y., Zhang, Y., 2020. Nanoscopic Visualization of Restricted Nonvolume Cholinergic and Monoaminergic Transmission with Genetically Encoded Sensors. Nano Letters 20, 4073-4083.

Supplementary Figure S1

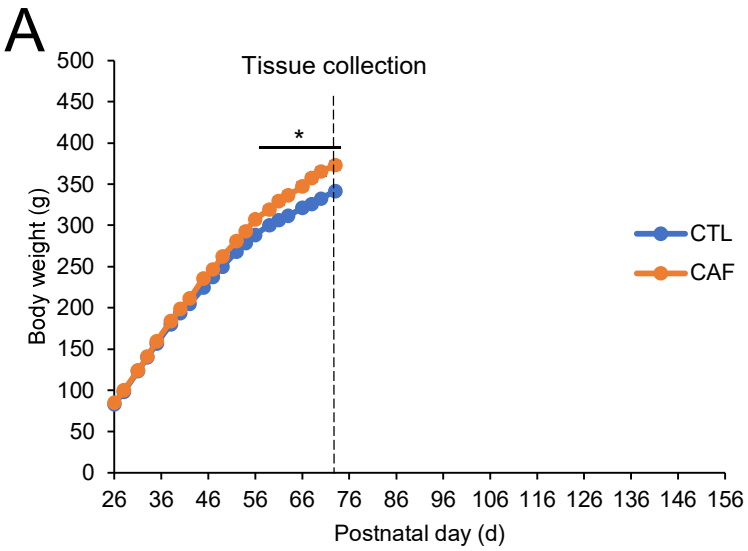

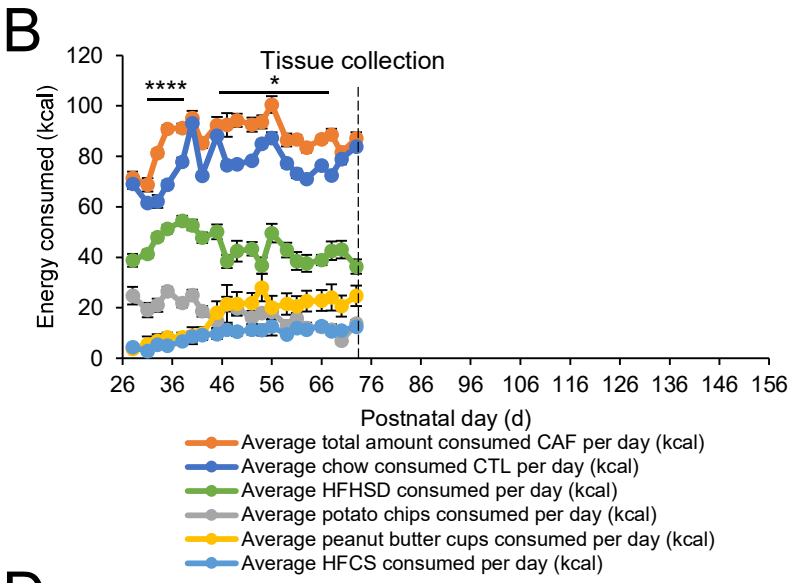

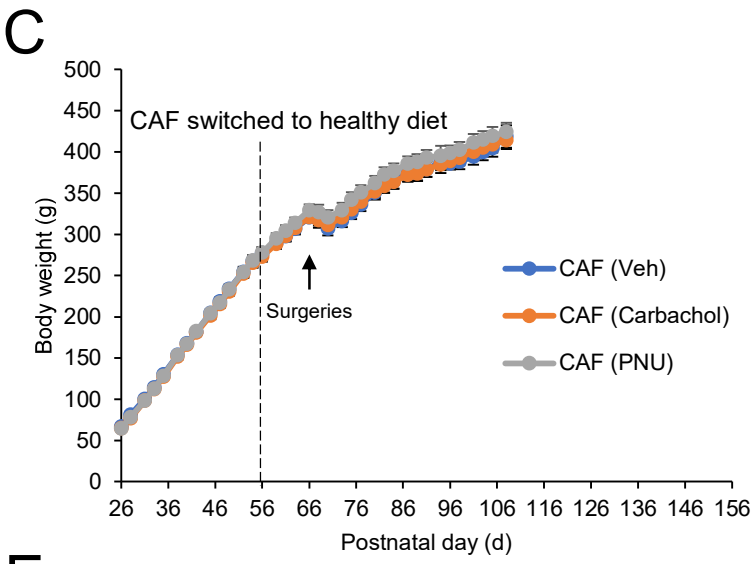

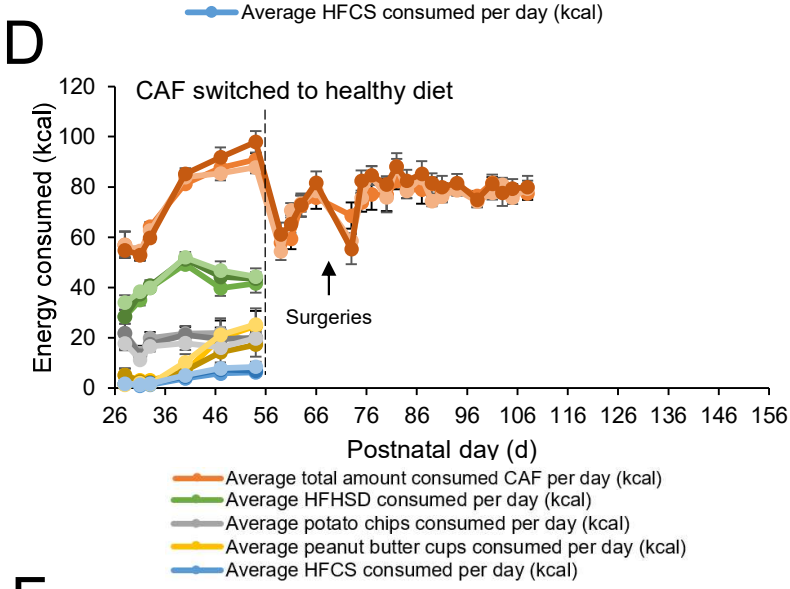

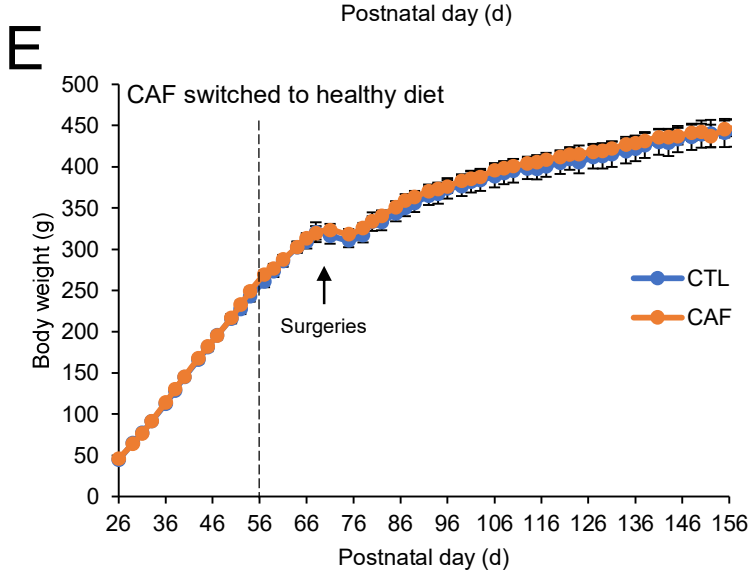

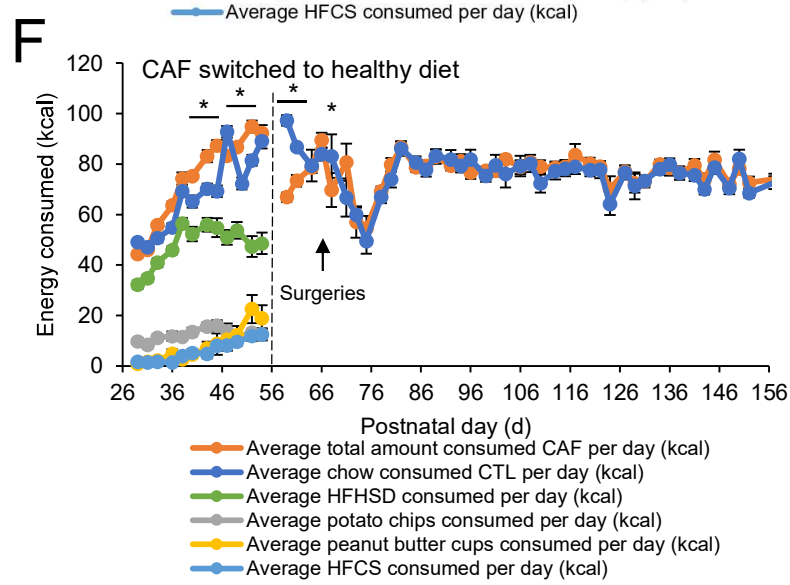

Supplementary Figure S1. Body weight and energy intake of subsequent experimental cohorts. (A) Body weight over time for tissue cohort with no healthy diet intervention. (B) Energy consumption over time for tissue cohort with no healthy diet intervention. (C) Body weight over time for acetylcholine receptor agonist cohort. (D) Energy consumption over time for acetylcholine receptor agonist cohort. (E) Body weight over time for in vivo fiber photometry cohort. (F) Energy consumption over time for in vivo fiber photometry cohort. CAF, cafeteria diet group; CTL, control group; HFCS, high-fructose corn syrup; HFHSD, high-fat high-sugar diet. Error bars represent ± SEM. *P<0.05, ****P<0.0001.

Supplementary Figure S2

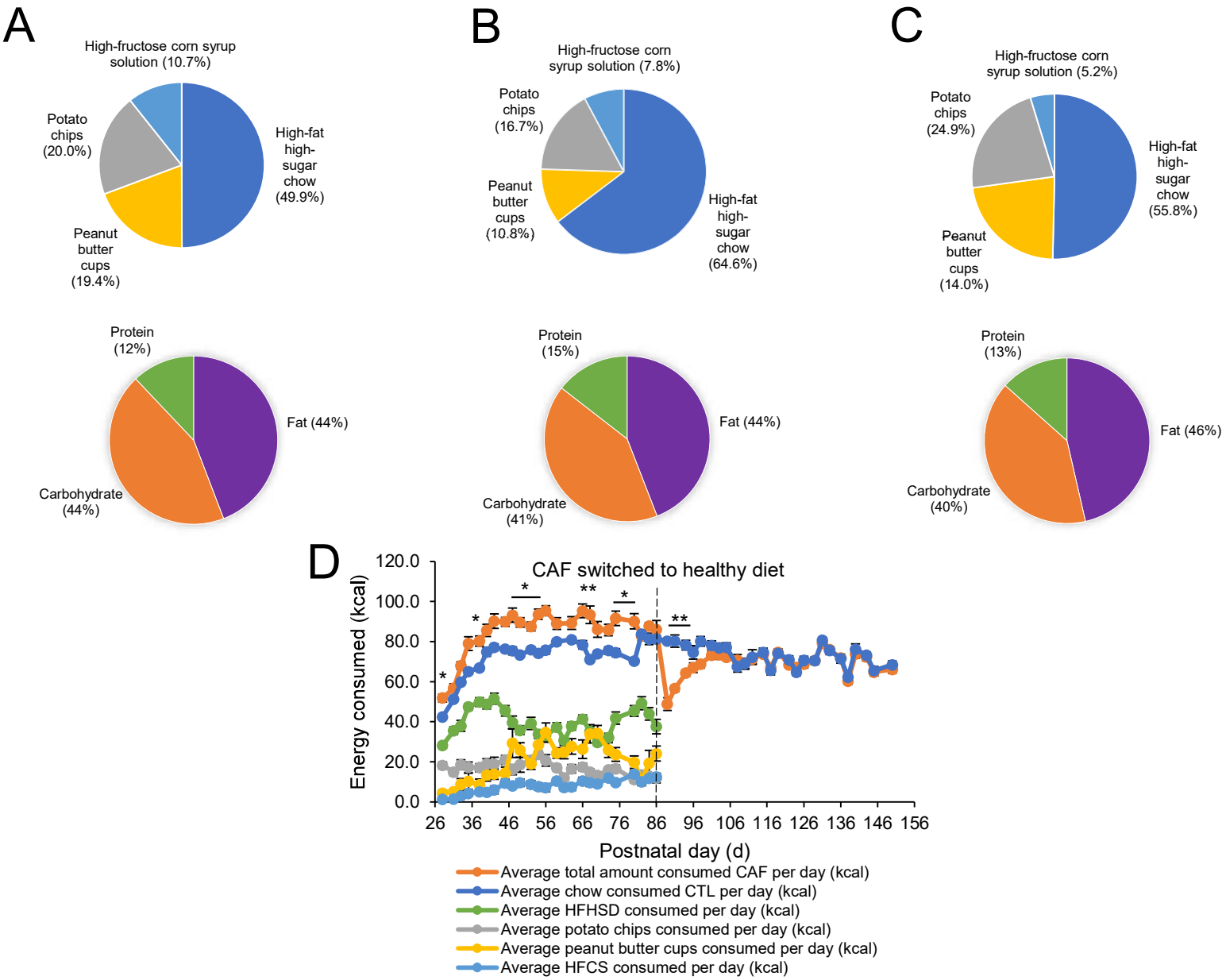

Supplementary Figure S2. (A-C) Breakdown of percentages of kilocalories consumed from the cafeteria diet components and macronutrients reveals consistency across cohorts. (E-F) No differences were observed for percent body fat or lean mass between CTL and CAF groups both before and after the healthy diet intervention period. CAF, cafeteria diet group; CTL, control group; HFCS, high-fructose corn syrup; HFHSD, high-fat high-sugar diet. Error bars represent ± SEM.

Supplementary Figure S3

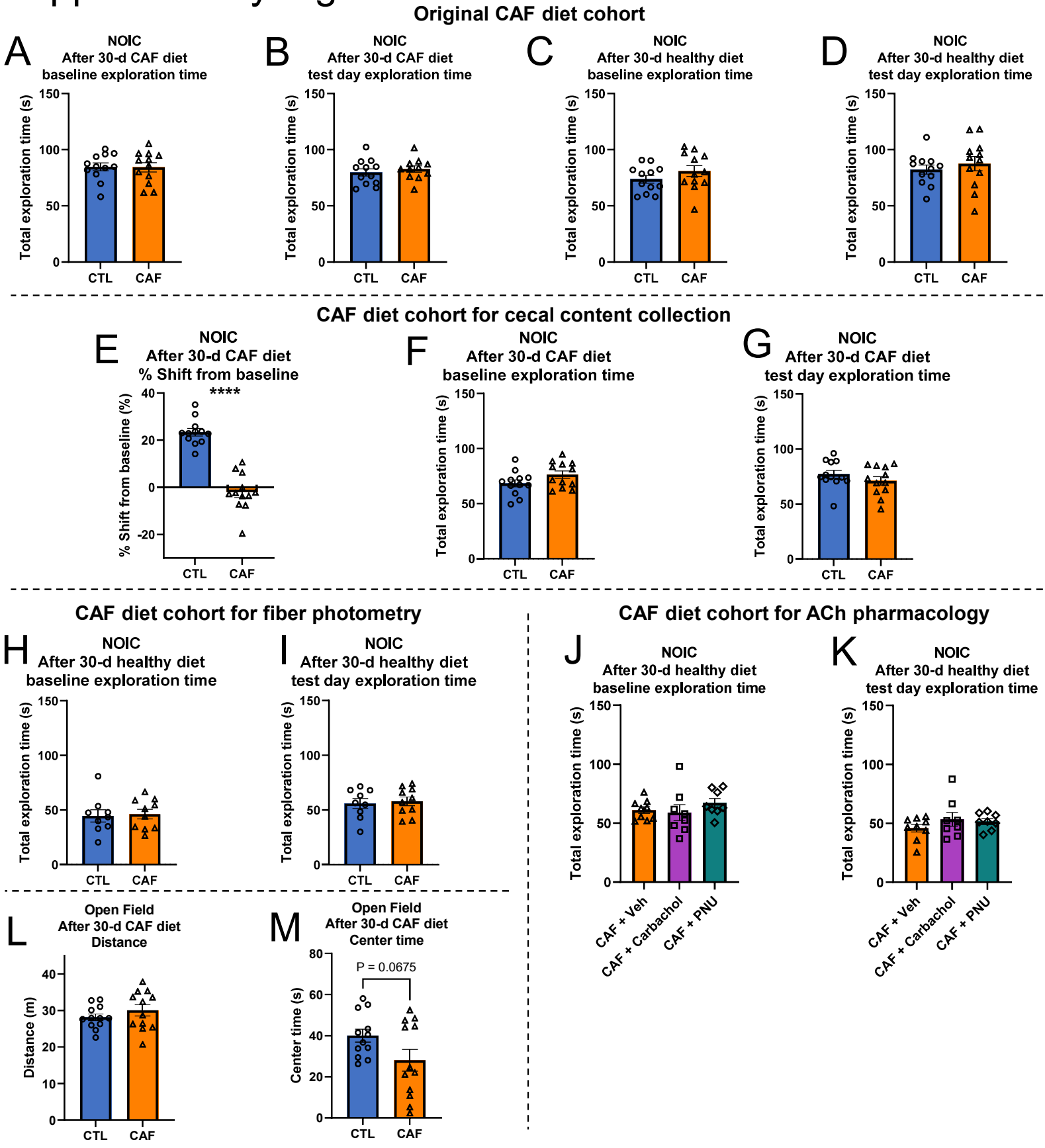

Supplementary Figure S3. (A-D, F-K) No differences in total object exploration time between the early life Western diet and control groups across cohorts, and (E) replication of hippocampal-dependent memory impairment in CAF cohort for tissue collection. (L-M) No differences observed in anxiety-like behavior and locomotor activity. CAF, cafeteria diet group; CTL, control group; Carbachol, general ACh agonist; NOIC, novel object in context; PNU, α7 nicotinic receptor agonist. Error bars represent ± SEM. ****P<0.0001.

Supplementary Figure S4

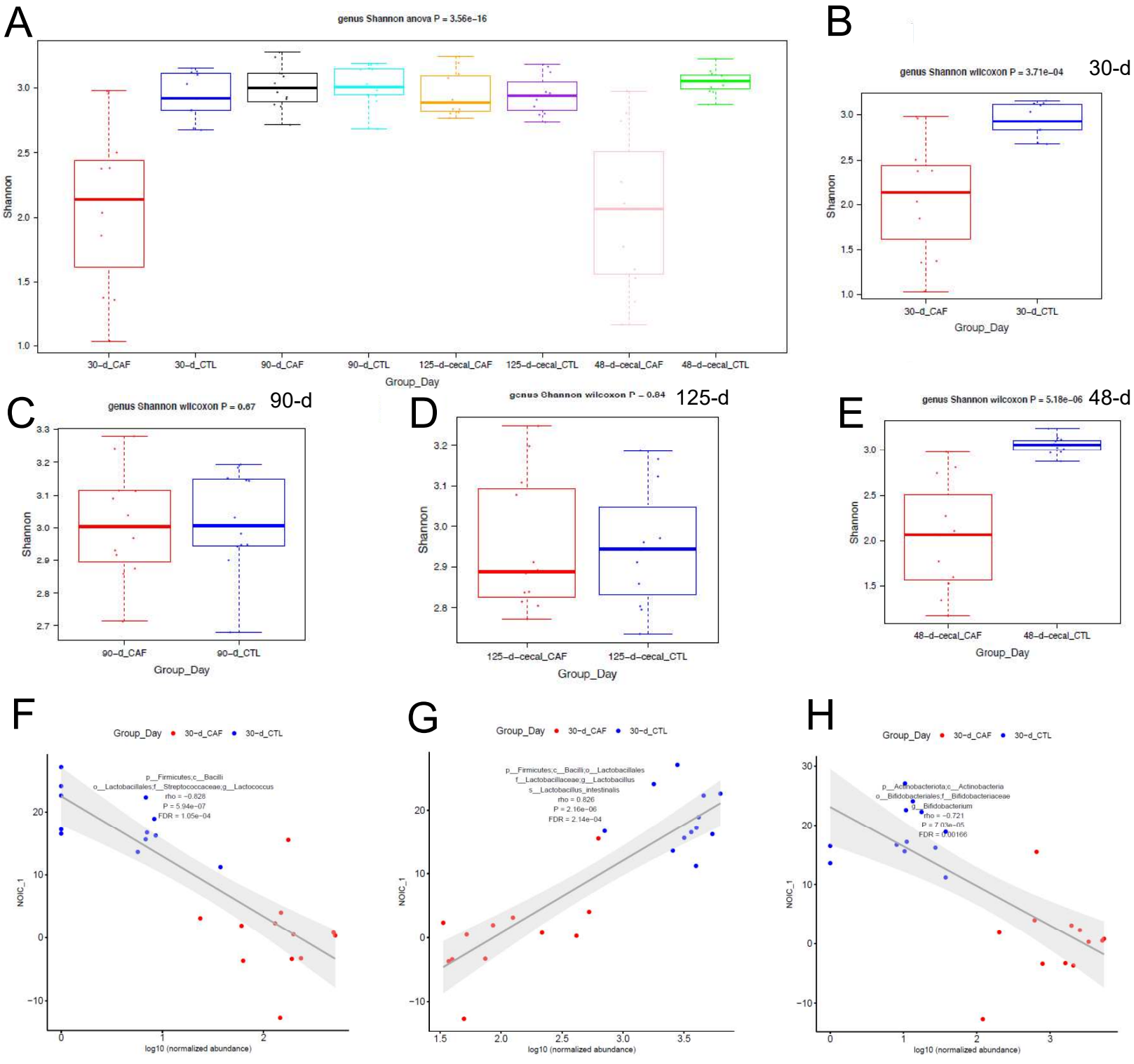

Supplementary Figure S4. Microbial diversity measures across time. (A) Shannon diversity indices in CAF vs. CTL groups at different time point. (B-E) Shannon diversity indices in CAF and CTL groups split per time point. (F-H) Correlational analyses between specific bacterial taxa and contextual episodic memory performance after the 30-d CAF diet period (but prior to the healthy diet intervention). CAF, cafeteria diet group; CTL control diet group; NOIC, Novel Object in Context. P-values are indicated in each subpanel.

Supplementary Figure S5

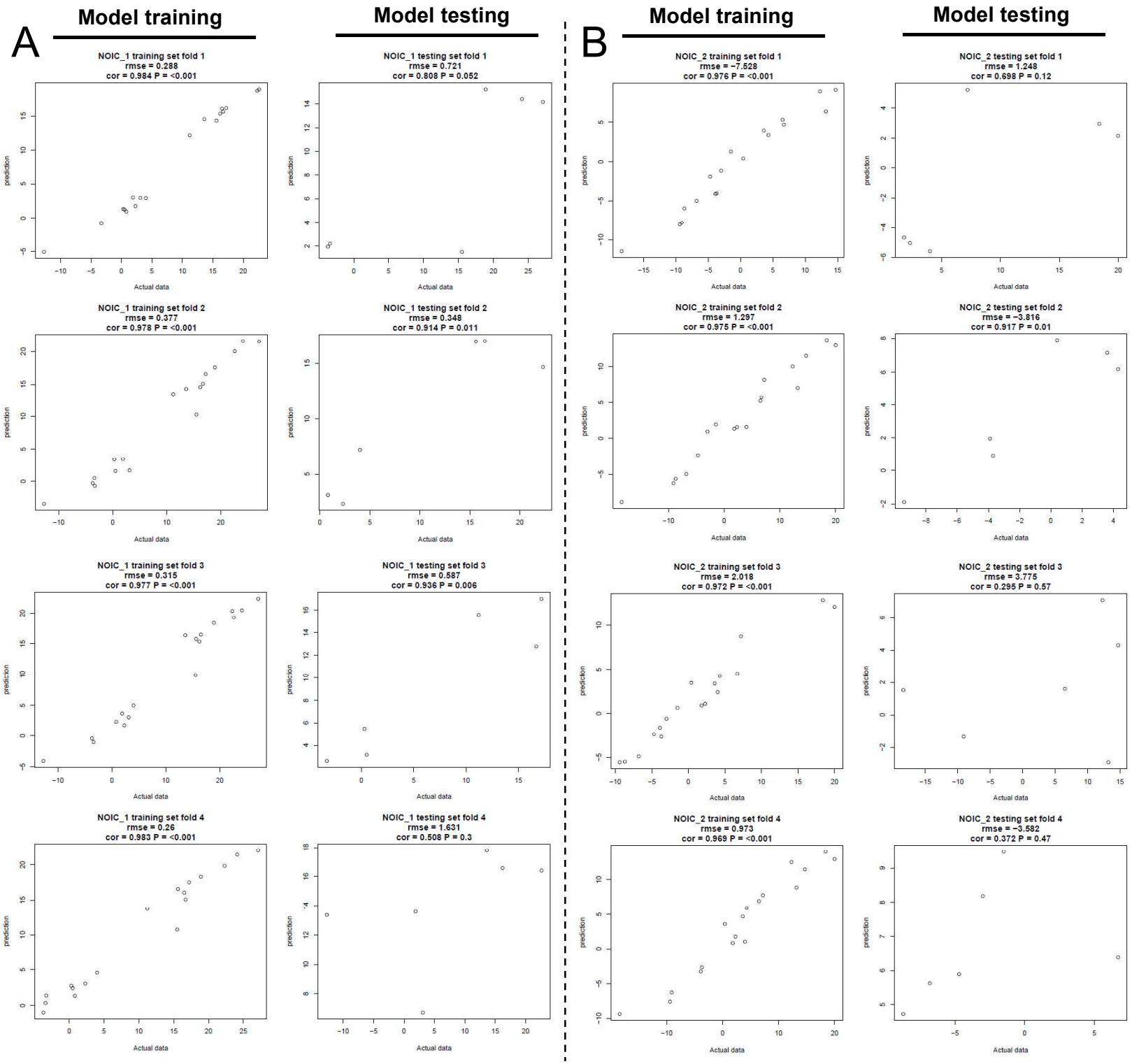

Supplementary Figure S5. Machine learning analyses further reveal that microbial taxonomic composition following the Western diet period does not predict memory performance after the heathy diet intervention period. (A) Machine learning analysis testing prediction of memory performance in NOIC before the healthy diet intervention period. (B) Machine learning analysis testing prediction of memory performance in NOIC after the healthy diet intervention period. CAF, cafeteria diet group; CTL control diet group; NOIC, novel object in context. P-values are indicated in each sub-panel.

Supplementary Figure S6

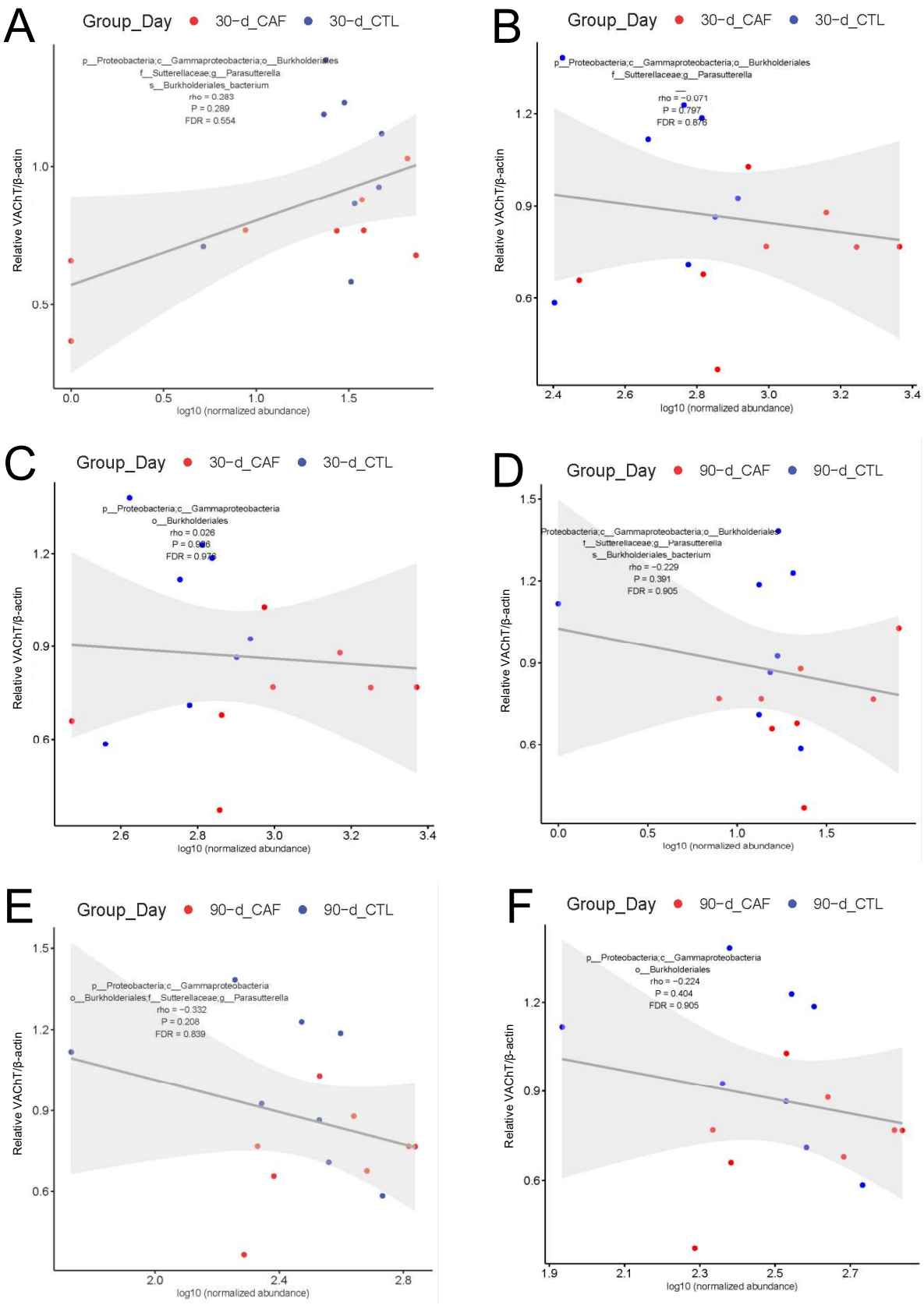

Supplementary Figure S6. (A-F) Correlations between microbial taxa and VAChT levels from immunoblotting before the healthy diet intervention period (30-d; A-C) and after the healthy diet intervention period (90-d; D-F). CAF, cafeteria diet group; CTL control diet group. P-values are indicated in each sub-panel.

Supplementary Figure S7

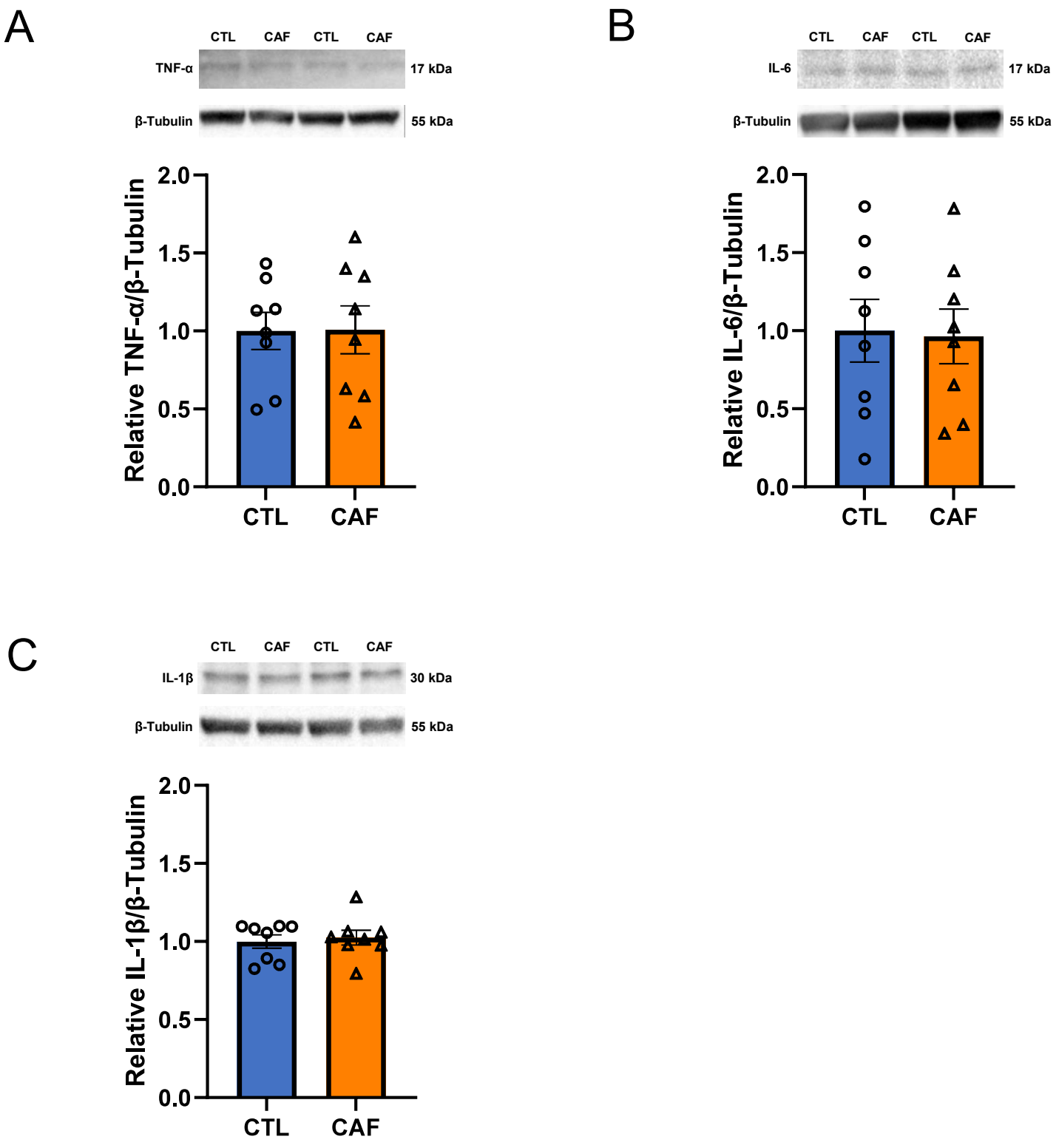

Supplementary Figure S7. Supplementary Figure S3. Levels of inflammatory cytokines in the dorsal hippocampus (HPCd) after the healthy diet intervention period. (**A**) Immunoblot representative images and results for tumor necrosis factor-α (TNF-α) protein levels in the dorsal hippocampus (HPC) of rats following WD access in early life and a healthy diet intervention in adulthood (N=16 total, n=8 CTL, n=8 CAF; paired t-test [2-tailed], P=0.97). (**B**) Immunoblot representative images and results for interleukin-6 (IL-6) protein levels in the dorsal hippocampus (HPC) of rats following WD access in early life and a healthy diet intervention in adulthood (N=16 total, n=8 CTL, n=8 CAF; paired t-test [2-tailed], P=0.89). (**C**) Immunoblot representative images and results for interleukin-1β (IL-1β) protein levels in the dorsal hippocampus (HPC) of rats following WD access in early life and a healthy diet intervention in adulthood (N=16 total, n=8 CTL, n=8 CAF; paired t-test [2-tailed], P=0.71). CAF, cafeteria diet group; CTL, control group; HPCd, dorsal hippocampus; IL-6, interleukin-6; IL-1β, interleukin-1β, TNF-α, tumor necrosis factor-α. Error bars represent ± SEM.

Supplementary Figure S8

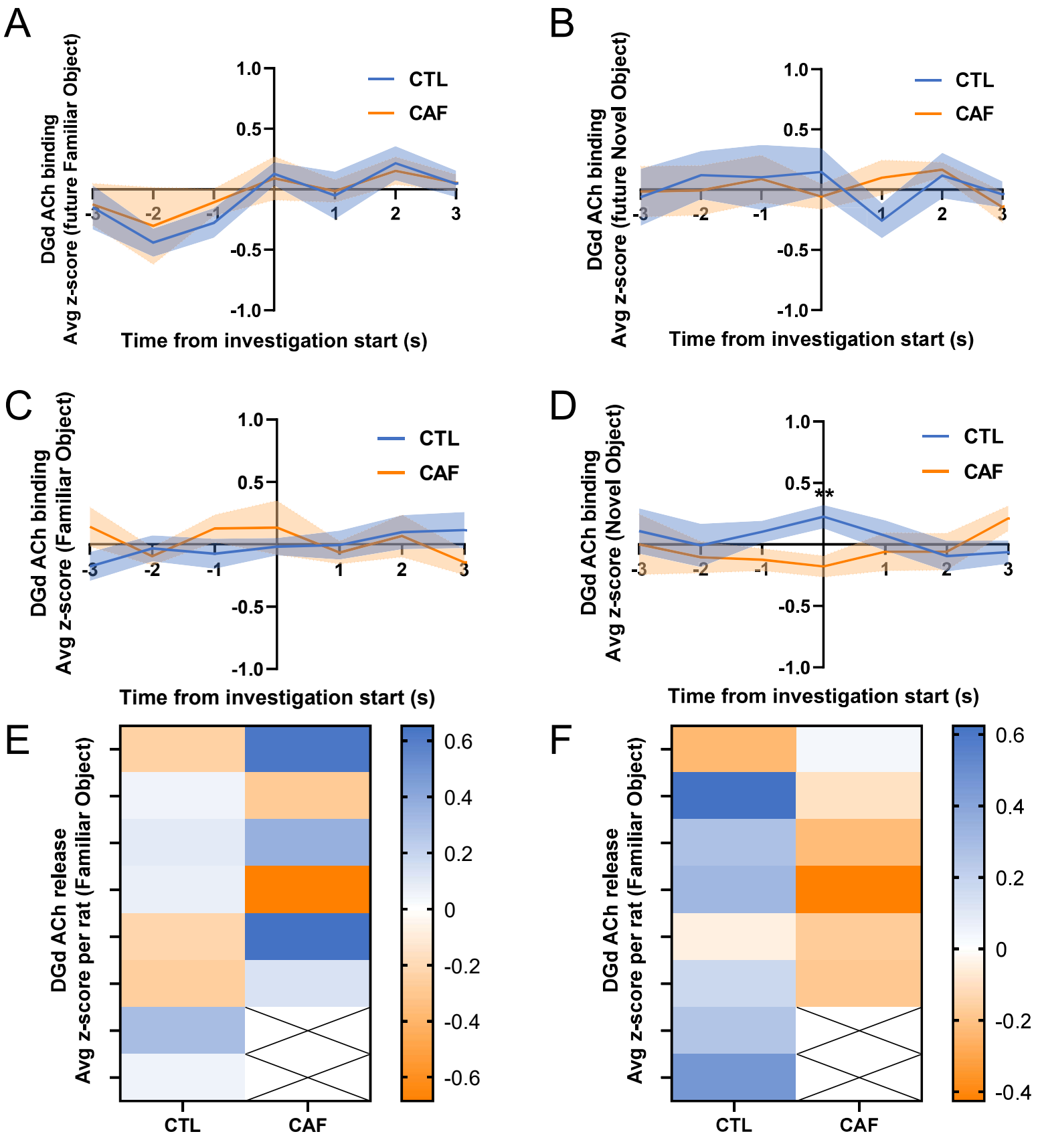

Supplementary Figure S8. Photometry analyses for hippocampus acetylcholine (ACh) release time-locked to investigations for baseline and test day object exploration in the contextual episodic memory task [Novel Object in Context, NOIC]. (A) ACh release over time during day 1 of NOIC for the future familiar object in context. (B) ACh release over time during day 1 of NOIC for the future novel object in context. (C) ACh release over time during day 3 of NOIC for the familiar object in context. (D) ACh release over time during day 3 of NOIC for the novel object in context. (E) Heat map of average z-score per rat at the initiation of an investigation for the familiar object in context (0 s). (F) Heat map of average z-score per rat at the initiation of an investigation for the novel object in context (0 s). ACh, acetylcholine; CAF, cafeteria diet group; CTL control diet group; NOIC, Novel Object in Context. Shading represents ± SEM for average values over time. **P<0.01.

Table S1. Number of subjects and statistical analyses used per experiment, summarized per main figure subpanel.

Figure and subpanel(s)	Number of subjects	Statistical analysis implemented	Statistical analysis results
1A	N/A	N/A	N/A
1B	24 total (n=12 CTL, n=12 CAF)	Two-way ANOVA (diet, time [as repeated measure], diet × time interaction)	diet × time: P=0.0004, no post hoc differences using Sidak's multiple comparisons test time: P<0.0001 diet: P=0.8772
1C-D	24 total (n=12 CTL, n=12 CAF)	Unpaired t-test (2-tailed)	C: P=0.0766 D: P=0.1834
1E-F	24 total (n=12 CTL, n=12 CAF)	Two-way ANOVA (diet, time [as repeated measure], diet × time interaction) for blood glucose over time; unpaired t-test (2-tailed) for blood glucose AUC	E: diet × time: P<0.0001, no post hoc differences using Sidak's multiple comparisons test time: P<0.0001 diet: P=0.3812 for AUC: P=0.3861 F: diet × time: P=0.8630 time: P<0.0001 diet: P=0.7111 for AUC: P=0.6909

1G-I	24 total (n=12 CTL, n=12 CAF)	Two-way ANOVA (diet, time [as repeated measure], diet × time interaction) for energy consumption over time; none for % kcal from the different CAF diet components and % kcal from macronutrients	diet × time: P<0.0001, many post hoc differences using Sidak's multiple comparisons test time: P<0.0001 diet: P=0.0479
2A, D, G, J	N/A	N/A	
2B	24 total (n=12 CTL, n=12 CAF)	Unpaired t-test (2-tailed) with Welch's correction for unequal variances	P=0.3258
2C, E-F	24 total (n=12 CTL, n=12 CAF)	Unpaired t-test (2-tailed) 2C (additional test): Two-way ANOVA (diet, NLR time point [as repeated measure], diet × NLR time point interaction) for memory performance over time	C (t-test): P<0.0001 C (ANOVA): diet × time point: P=0.0589, post hoc differences using Sidak's multiple comparisons test, CTL: P=0.0044, CAF: 0.7727 diet: P=0.0021 time point: 0.0081 E: P<0.0001 F: P=0.002
2H-I	24 total (n=12 CTL, n=12 CAF)	Unpaired t-test (2-tailed)	H: P=0.3320 I: P=0.0634
2K	23 total (n=11 CTL due to outlier, n=12 CAF)	Unpaired t-test (2-tailed)	P=0.4064 for % time in open P=0.1175 for entries into open

2L	23 total (n=12 CTL, n=11 CAF due to outlier)	Unpaired t-test (2-tailed)	P=0.7719 for % time in open P=0.6752 for entries into open
3A	24 total (n=12 CTL, n=12 CAF)	See microbiome analyses section	FDR<0.1 for significant taxa
3B-E	24 total (n=12 CTL, n=12 CAF)	Bray-Curtis dissimilarity for genus level abundance with PCoA	P<0.05 for significant associations B: R^2=0.56214, P=0.001 C: R^2=0.04465, P=0.388 D: R^2=0.61842, P=0.001 E: R^2=0.0749, P=0.388
3F	24 total (n=12 CTL, n=12 CAF)	See machine learning analysis section; random forest regression models	For training data: Cor 0.983 and P=2.83e-35 Cor 0.97 and P=2.83e-35 For testing data: Cor 0.591 and P=0.002; Cor 0.04 and P=0.854
4A	15 total (n=7 CTL due to outlier, n=8 CAF)	Unpaired t-test (2-tailed)	P=0.9165
4B	16 total (n=8 CTL, n=8 CAF)	Unpaired t-test (2-tailed)	P=0.0449
4C	15 total (n=8 CTL, n=7 CAF due to outlier)	Unpaired t-test (2-tailed)	P=0.5570
5A-C	N/A	N/A	N/A

5D	18 total (n=9 CTL, n=9 CAF)	Unpaired t-test (2-tailed)	P=0.0064
5E	8 total (n=8 CTL group only)	Paired t-test (2-tailed); two-way ANOVA (diet, object [as repeated measure], diet × object interaction) for additional analysis	t-test: P=0.0140 two-way ANOVA: object × diet: P=0.0087, no post hoc differences using Sidak's multiple comparisons test (P=0.1111 comparing objects within CTL group, P=0.0758 comparing objects within CAF group) object: P=0.7119 diet: P=0.3960
5F	6 total (n=6 CAF group only)	Paired t-test (2-tailed); same two-way ANOVA analysis as in 5D	t-test: P=0.1453 two-way ANOVA: same results as in 5D
5G-H	14 total (n=8 CTL, n=6 CAF)	Unpaired t-test (2-tailed); two-way ANOVA (diet, object [as repeated measure], diet × object interaction) for additional analysis	F (t-test): P=0.0068 G (t-test): P=0.4641 F and G (two-way ANOVA): object × diet: P=0.0087, post hoc differences using Sidak's multiple comparisons test (P=0.0478 for novel object between diet groups, P=0.6038 for familiar object between diet groups) object: P=0.7119 diet: P=0.3960

5I	14 total (n=8 CTL, n=6 CAF)	Simple linear regression	$R^2 = 0.63$ P=0.0006
5J	8 total (n=8 CTL group only)	Simple linear regression	$R^2 = 0.57$ P=0.02
5K	6 total (n=6 CAF group only)	Simple linear regression	$R^2 = 0.27$ P=0.28
6A-B	N/A	N/A	N/A
6C	25 total (n=9 CAF+Vehicle, n=8 CAF+Carbachol, n=8 CAF+PNU due to outliers)	One-way ANOVA (infusion group) with Tukey's post-hoc test for multiple comparisons	$F_{(2,22)} = 5.122$ and P=0.0149 for overall model and for multiple comparisons: CAF+Vehicle vs. CAF+Carbachol: P=0.0226 CAF+Vehicle vs. CAF+PNU: P=0.0431 CAF+Carbachol vs. CAF+PNU: P=0.9542

ANOVA, analysis of variance; AUC, area under the curve; CAF, cafeteria diet group; CTL, control group; PNU, PNU 282987 (α7 nicotinic receptor agonist).